

Cite this article as: Hu Jianhua, Liang Xiaoyuan, Ding Xiaofeng, et al. Numerical Simulation of Microstructure Evolution of AZ31 Magnesium Alloy Tube During Two-High Rotary Piercing[J]. Rare Metal Materials and Engineering, 2022, 51(09): 3244-3251.

ARTICLE

Numerical Simulation of Microstructure Evolution of AZ31 Magnesium Alloy Tube During Two-High Rotary Piercing

Hu Jianhua¹, Liang Xiaoyuan², Ding Xiaofeng³, Shuang Yuanhua¹, Wang Qinghua⁴

¹ College of Materials Science and Engineering, Taiyuan University of Science and Technology, Taiyuan 030024, China; ² School of Materials Science and Engineering, Northwestern Polytechnical University, Xi'an 710072, China; ³ Shanxi Provincial Key Laboratory of Metallurgical Equipment Design Theory and Technology, Taiyuan University of Science and Technology, Taiyuan 030024, China; ⁴ School of Electronic Information Engineering, Taiyuan University of Science and Technology, Taiyuan 030024, China

Abstract: A new piercing method (two-high rotary piercing) for magnesium alloy seamless pipes was proposed, and the two-high piercing process was simulated by DEFORM-3D finite element analysis software. Results show that the simulated microstructures and the experiment ones all exhibit the similar evolution rules, and their average grain sizes are close to each other's, suggesting that the two-high piercing process is a feasible method to pierce AZ31 magnesium alloy seamless tubes and the DEFORM-3D software is a reliable tool to simulate the two-high piercing process.

Key words: magnesium alloy seamless tube; two-high rotary piercing; numerical simulation; microstructure evolution

Magnesium alloy has been widely used in many fields due to its low density, high electrical and thermal conductivities, excellent machinability, and damping property. The Mg alloys are commonly used in seamless pipe production in aerospace, fluid pipeline, and high-speed rail industries^[1-3].

The extrusion, drawing, and rolling are three major processing methods of magnesium alloy seamless pipes. Among them, the rolling method has the advantages of high production efficiency and low cost, therefore attracting extensive attention in recent years. Guo et al^[4] simulated the three-high rotary piercing process, and found that the suitable deformation temperature for the stable skew rolling of AZ31B magnesium alloy is 350 °C. Lin et al^[5] simulated the three-high tandem skew rolling process of AZ31 magnesium alloy by DEFORM-3D finite element software. Ding et al^[6] successfully prepared the small-size seamless tubes of AZ31 magnesium alloy by three-high tandem skew rolling, and the microstructure size of the seamless tubes was refined to 3 μm. Sun et al^[7] used three-high rotary piercing method to produce the large-size magnesium alloy pipe, and found that at 500 °C, the axial and longitudinal microstructures of rolled pieces are more uniform, the wall thickness is more stable, and all the

pipe properties are improved.

According to the above-mentioned research, it is clear that the three-high rotary piercing process is the major method to produce magnesium alloy seamless pipes^[8]. However, during the production process, the defect of tail triangle is inevitable^[9]. But this defect may not form when the magnesium alloy seamless pipes are produced by two-high piercing process since the deformation zone of two-high piercing mill consists of two guide shoes. Therefore, the two-high piercing process is likely to be a potential method to produce magnesium alloy seamless pipes.

In this research, the SolidWorks software was used to establish the spatial geometry model and the DEFORM-3D finite element software was used to simulate the two-high piercing process. The microstructure evolution during the whole piercing process was analyzed. The simulated results were also compared with the experiment ones.

1 Geometric Model of Two-High Rotary Piercing

The two-high piercing process has been widely used in the field of steel pipe production. Theoretically, the process is more beneficial for metal flow and to reduce harmful

Received date: September 03, 2021

Foundation item: Shanxi Province Key Technology Project (20191102009); Shanxi Province Key Project of Research and Development Plan (201903D121049)

Corresponding author: Hu Jianhua, Ph. D., Associate Professor, College of Materials Science and Engineering, Taiyuan University of Science and Technology, Taiyuan 030024, P. R. China, E-mail: 2005022@tyust.edu.cn

Copyright © 2022, Northwest Institute for Nonferrous Metal Research. Published by Science Press. All rights reserved.

deformation^[10].

Fig. 1 shows the geometrical model of two-high rotary piercing. Each roll consisted of an inlet cone and an outlet cone. These two cones were linked by transition belt, and the diameter of the roll gradually increased. During the rolling process, the billet suffered from the resistance of the plug. The metal flow speed was increased with increasing the axial roll speed, which reduced the inhomogeneous deformation, circumferential shear stress, and the useless deformation of capillary. In addition, the generation of cavity was inhibited, the quality of capillary was improved, and the inner and outside surface defects of capillary were reduced^[11].

The small roll surface cone angle was adopted in this model since it could reduce slip, thereby increasing the deformation area and the friction drag on the contact surface of the roll inlet cone and reducing the axial positive pressure. The entrance cone angle, exit cone angle, feed angle, and rolling angle were 2.5°, 3.0°, 10.0°, and 15.0°, respectively.

2 Finite Element Model of AZ31 Magnesium Alloy During Two-High Piercing

Based on Ref. [9], the rolling temperature of magnesium alloy tube in rotary piercing process was 300~400 °C. Since the deformation temperature range of magnesium alloy was relatively small, it was necessary to preheat the magnesium alloy before contact with the cold die to prevent the cracking.

The constitutive equation of the material used in this research is as follows:

$$\dot{\epsilon} = 1.494 \times 10^{11} \left[\sinh(0.21\sigma) \right]^{6.24} \exp\left(-\frac{177200}{RT}\right) \quad (1)$$

where $\dot{\epsilon}$ is strain rate (s^{-1}), σ is true stress (MPa), R is the universal gas constant ($8.314 \text{ J} \cdot \text{mol}^{-1} \cdot \text{K}^{-1}$), and T is the absolute temperature (K).

To increase the accuracy of the simulation, the parameters of AZ31 magnesium alloy, such as Young's modulus, thermal conductivity, and specific heat capacity, were considered as variables depending on temperature. Fig. 2 presents the variation of Young's modulus with increasing the temperature. The Young's modulus of magnesium alloy is decreased with increasing the temperature^[12].

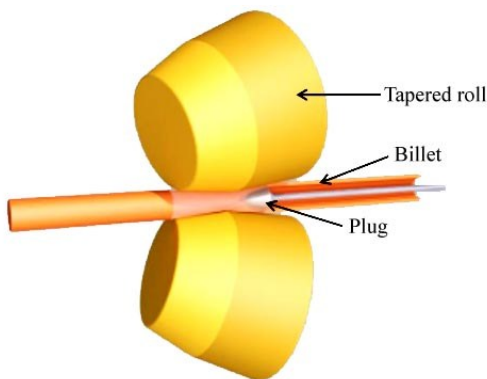


Fig.1 Schematic diagram of two-high rotary piercing geometrical model

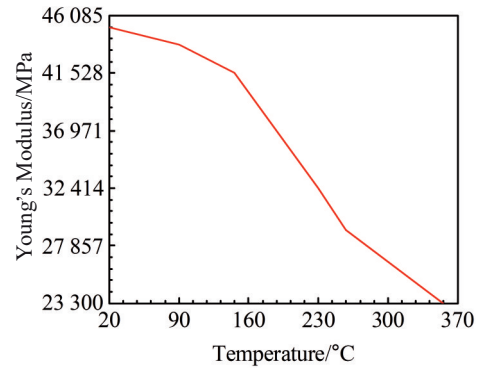


Fig.2 Relationship between Young's modulus and temperature

In the piercing process, the frictional heating of the rolled piece with the plug, roll, and guide shoes is very serious, particularly the one between the plug and the billet. Therefore, the accurate thermal conductivity has a great influence on the simulation results^[12]. Fig. 3 displays the variation of thermal conductivity with different temperatures. It is clear that the thermal conductivity of magnesium alloy is increased with increasing the temperature.

The specific heat capacity of AZ31 magnesium alloy is also increased linearly with increasing the temperature, as expressed by Eq.(2), as follows:

$$F = 7.88 \times 10^5 T + 1.004 \times 10^9 \quad (2)$$

where F is the specific heat capacity ($\text{J} \cdot \text{kg}^{-1} \cdot \text{K}^{-1}$).

In addition, the coefficient of heat radiation was set as 0.45, and the diffusion coefficient was 0.12.

The finite element model is shown in Fig. 4. The deformation tools are regarded as rigid bodies, and the billet is a deformation body, which is divided into 50 000 tetrahedral elements.

Assuming that the friction between the billet and rolling tools conforms to the constant shear stress, the plastic shear model was adopted. The friction coefficients between the billet and different deformation tools are different: the friction coefficients between roll and the tube, between guide shoes and the billet, and between the plug and the billet are 1.68, 0.3, and 0.7, respectively. The speed boundary condition was employed, the roll speed was 230 r/min. The initial

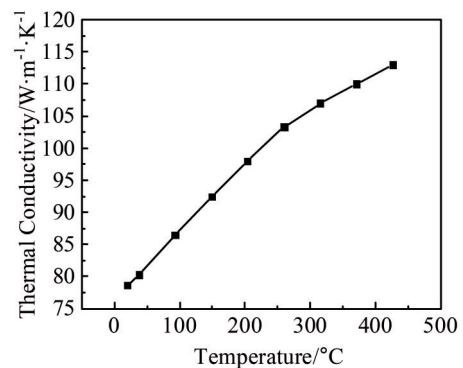


Fig.3 Relationship between thermal conductivity and temperature

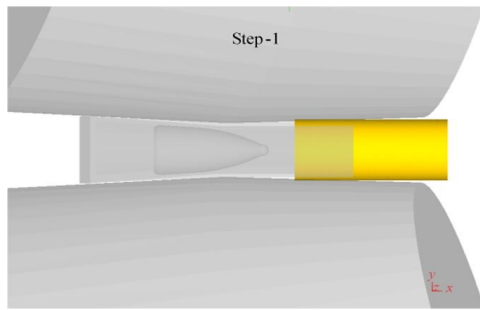


Fig.4 Schematic diagram of finite element model of two-high rotary piercing

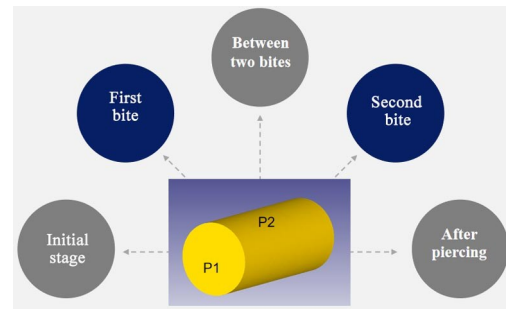


Fig.5 Deformation stages of AZ31 magnesium alloy during piercing process

temperature of the billet was 350 °C, and the preheating temperature of rolling tool was 330 °C.

3 Results and Discussion

In order to investigate the microstructure evolution of AZ31 magnesium alloy during the whole piercing process, a couple of points were selected to observe the microstructures at different deformation stages^[13], as shown in Fig.5. There are five stages: initial stage, first bite stage, between-two-bites stage, second bite stage, and after-the-piercing stage. Two points were selected on the blank surface. Point 1 (P1) is at the center of the cross section, and point 2 (P2) is on the outside surface of the blank near the entrance.

3.1 Microstructure evolution

The grain sizes, microstructures, and grain boundary misorientations of the tube billet in the initial stage are shown

in Fig. 6. It can be seen that the microstructures consist of coarse grains. At P1, the minimum, maximum, and average grain sizes are 20.867, 29.705, and 24.984 μm , respectively. At P2, the minimum, maximum, and average grain sizes are 20.653, 31.474, and 24.911 μm , respectively. Obviously, the grain sizes at the center and on the outside surface of billet are similar. Moreover, the maximum or minimum grain boundary misorientations at P1 and P2 are the same with standard deviations of 0° and 37.753° for P1 and P2, respectively.

Fig. 7 shows the grain sizes, microstructures, and grain boundary misorientations at P1 and P2 during the first bite stage. The dynamic recrystallization occurs at both points, and it is obvious that small new grains are formed at the original grain boundaries. Moreover, the new grains formed on the outside surface of the billet grow faster than those at the billet center do. The minimum, maximum, and average grain sizes at P1 are 1.128, 38.613, and 5.760 μm , respectively. The

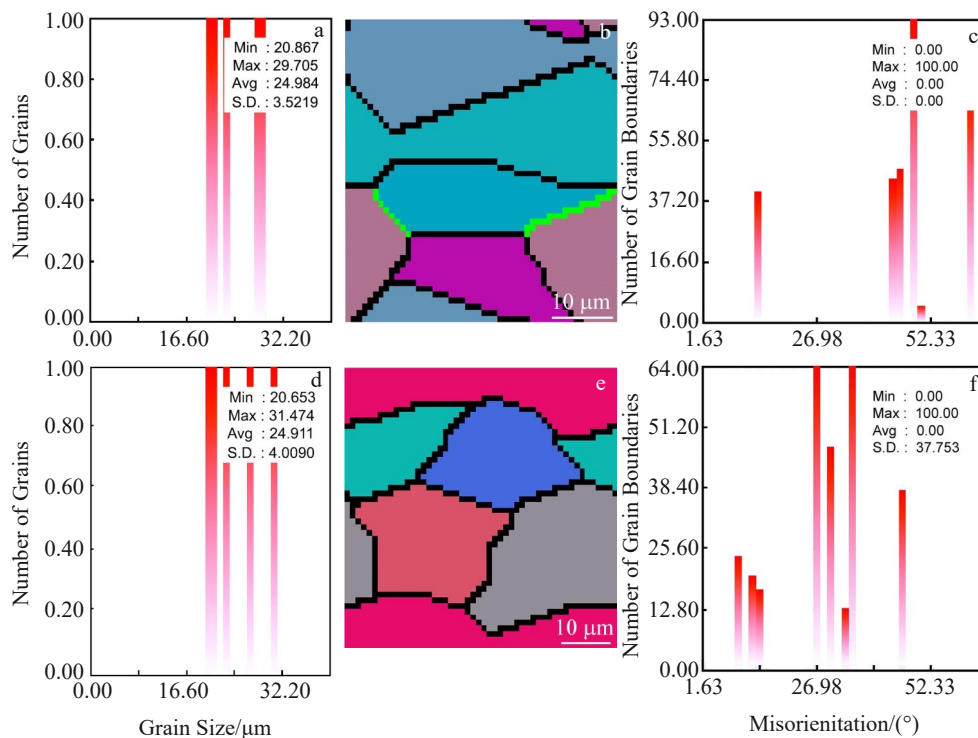


Fig.6 Grain sizes (a, d), microstructures (b, e), and grain boundary misorientations (c, f) of P1 (a-c) and P2 (d-f) points at initial stage

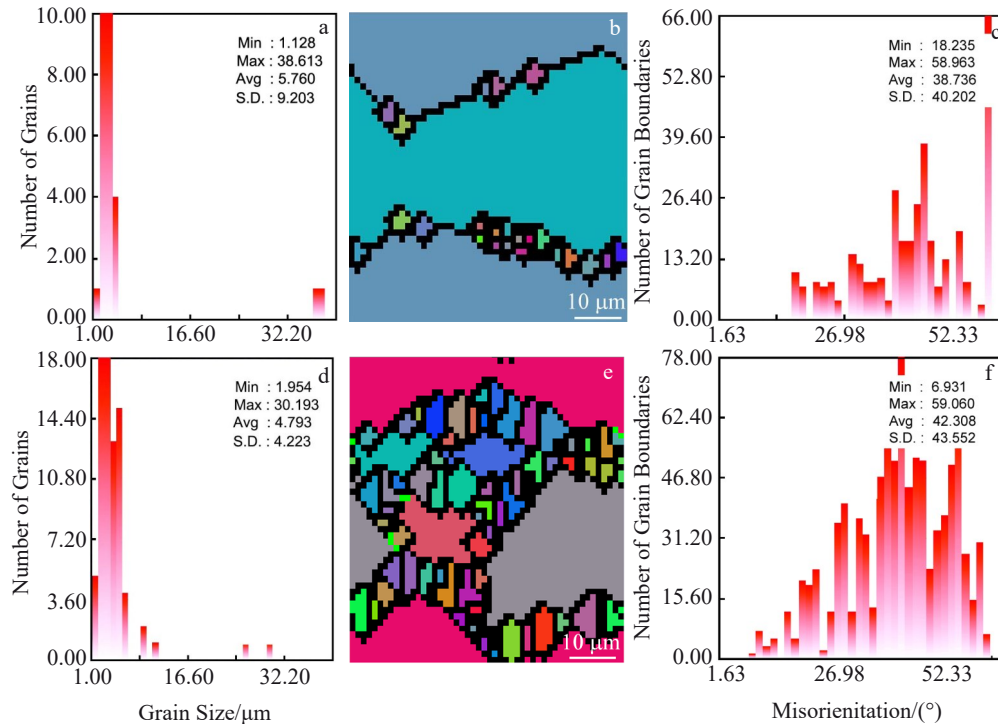


Fig.7 Grain sizes (a, d), microstructures (b, e), and grain boundary misorientations (c, f) of P1 (a~c) and P2 (d~f) points during the first bite stage

minimum, maximum, and average grain sizes at P2 are 1.954, 30.193, and 4.793 μm , respectively. In the first bite stage, the deformation on the outside surface of the billet is greater than that at the center. In addition, the minimum grain boundary misorientation at P1 is 18.235°, which is much greater than 10°, indicating that there is only high-angle grain boundaries at P1; while the minimum grain boundary misorientation on the outside surface is 6.931°, which is smaller than 10°, indicating that the small-angle grain boundaries exist at P2.

Fig. 8 presents the grain sizes, microstructures, and grain boundary misorientations at P1 and P2 at the between-two-bites stage. It is clear that the minimum, maximum, and average grain sizes at P1 are 5.171, 25.953, and 9.815 μm , respectively. The minimum, maximum, and average grain sizes at P2 are 1.128, 11.780, and 5.070 μm , respectively. Therefore, it can be concluded that in the two-high rotary piercing process, the new recrystallized grains form constantly and then grow. The grain size on the outside surface of the billet is smaller than that at the billet center, indicating that the deformation degree on the outside surface is greater at this stage. Furthermore, the minimum grain boundary misorientation is 18.235° at P1, which indicates that at the billet center, all grain boundaries are high-angle grain boundaries. Although the minimum grain boundary misorientation is 6.931° at P2, the grain boundary misorientations of >14.3° account for a large proportion, inferring that the majority are high-angle grain boundaries.

Fig. 9 displays the grain sizes, microstructures, and grain boundary misorientations at P1 and P2 at the second bite stage. It can be found that the minimum, maximum, and

average grain sizes at P1 are 1.128, 18.472, and 3.223 μm , respectively. The minimum, maximum, and average grain sizes at P2 are 1.128, 8.291, and 4.074 μm , respectively. The grain sizes in this stage are obviously smaller than those in the previous step, because the piercing plug is brought into contact with the billet, which increases the deformation degree at the center and on the outside surface of the billet and then leads to the decrease in grain size. It is obvious that the original grains are gradually replaced by new grains.

Moreover, the minimum and maximum grain boundary misorientations at P1 are 4.154° and 60.487°, respectively. The minimum and maximum grain boundary orientations at P2 are 1.866° and 61.429°, respectively. Because most grain boundary orientations are greater than 14.3°, the high-angle grain boundaries account for a large proportion and they continuously change, which confirms the occurrence of dynamic recrystallization.

Fig. 10 demonstrates the grain sizes, microstructures, and grain boundary misorientations at P1 and P2 after the second bite stage. The minimum, maximum, and average grain sizes at P1 are 1.128, 10.645, and 4.093 μm , respectively. The minimum, maximum, and average grain sizes at P2 are 1.128, 9.027, and 4.252 μm , respectively. In addition, it is clear that the grain shape is relatively uniform at P1 and the grain size is smaller than that after the first bite stage. The newly recrystallized grains at P2 are formed at the grain boundaries. Meanwhile, with increasing the deformation degree, the recrystallized grains grow slowly and gradually replace the original grains.

It can be also observed from Fig.10 that the minimum grain

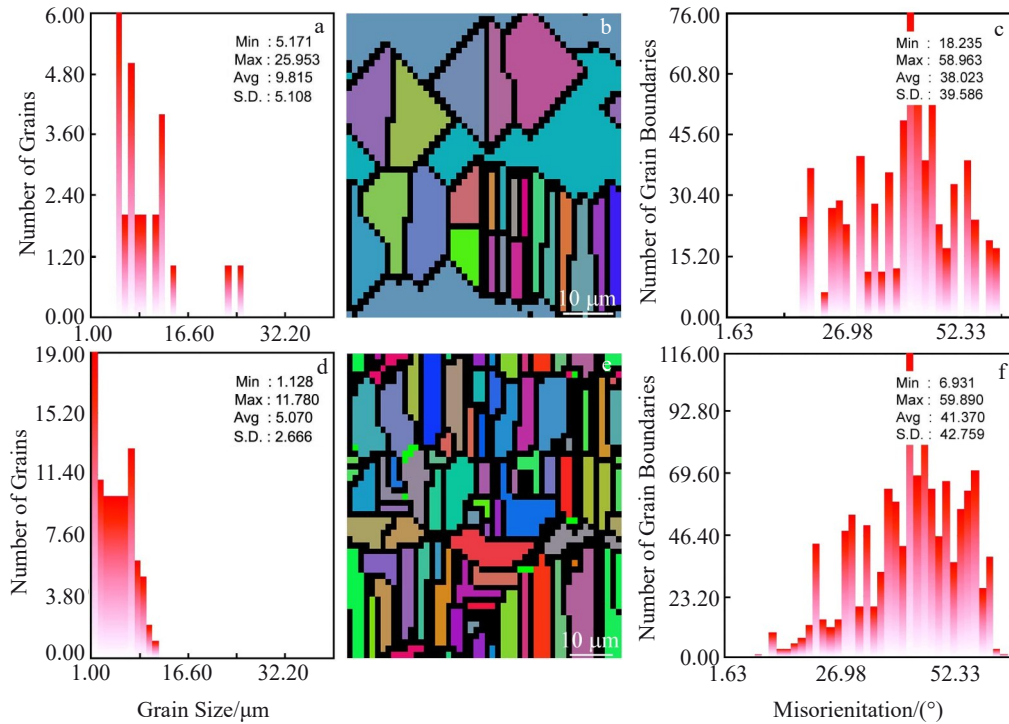


Fig.8 Grain sizes (a, d), and microstructure distributions (b, e), and grain boundary misorientations (c, f) of P1 (a~c) and P2 (d~f) points during the between-two-bites stage

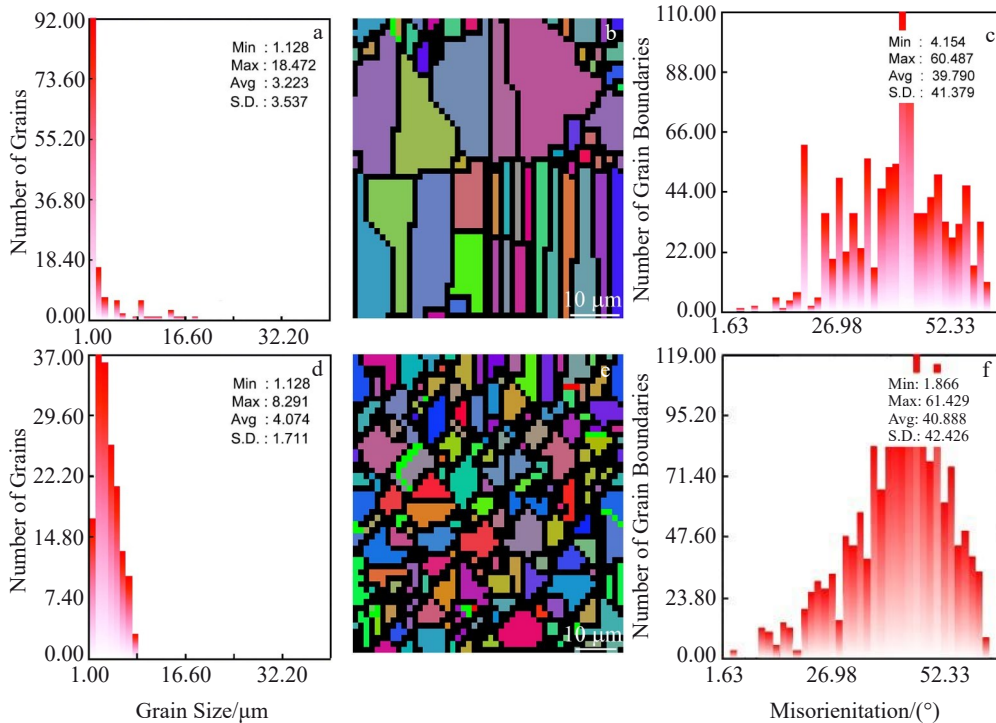


Fig.9 Grain sizes (a, d), microstructures (b, e), and grain boundary misorientations (c, f) of P1 (a~c) and P2 (d~f) points at the second bite stage

boundary misorientation at P1 is 7.147° and few grain boundaries have the misorientations less than 10° , indicating that few low-angle grain boundaries exist at the billet center. The minimum grain boundary orientation at P2 is 14.475° ,

indicating that all grain boundaries on the outside surface of the tube billet are high-angle grain boundaries.

Fig. 11 shows the grain sizes, microstructures, and grain boundary misorientations at P1 and P2 after piercing. The

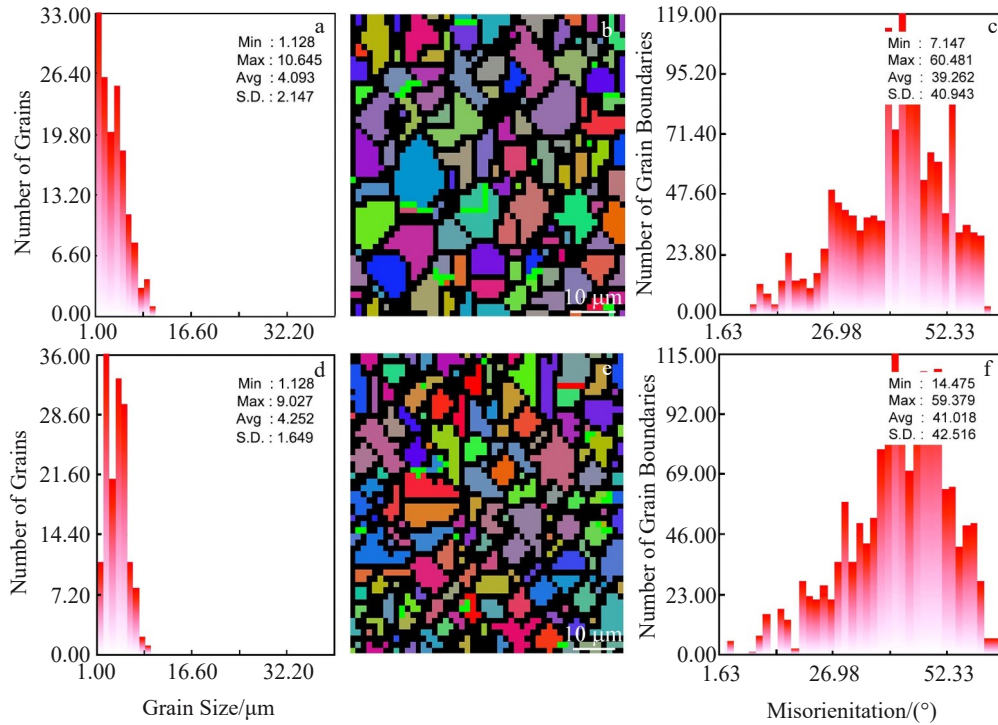


Fig.10 Grain sizes (a, d), microstructures (b, e), and grain boundary misorientations (c, f) of P1 (a~c) and P2 (d~f) points after the second bite stage

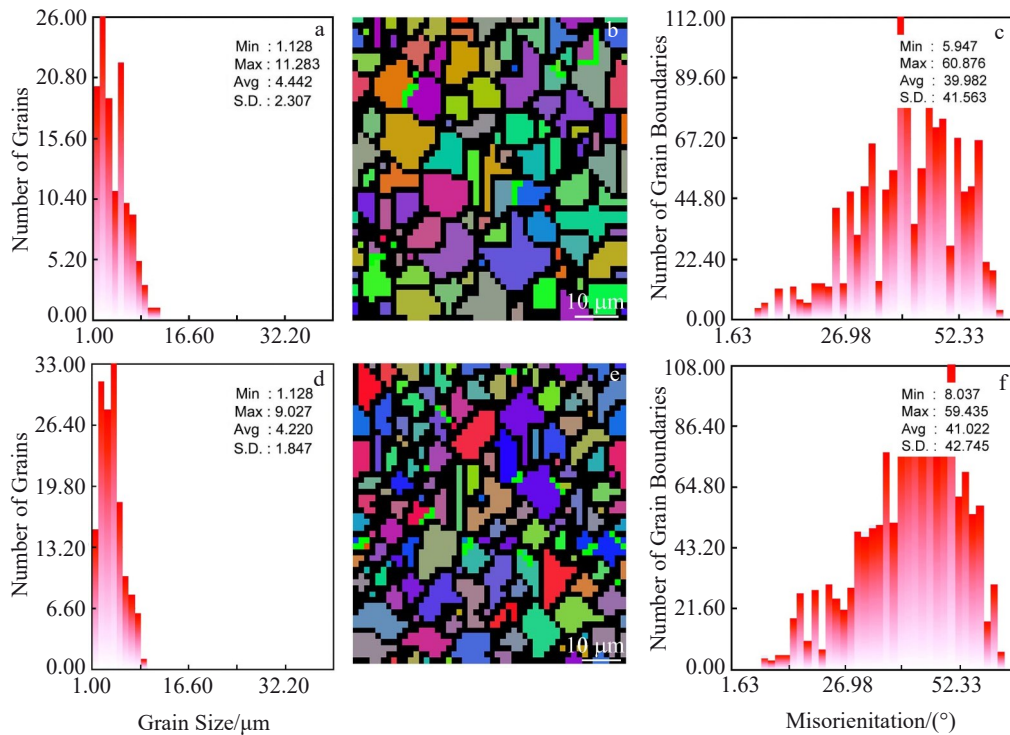


Fig.11 Grain sizes (a, d), microstructures (b, e), and grain boundary misorientations (c, f) of P1 (a~c) and P2 (d~f) points after piercing process

minimum, maximum, and average grain sizes at P1 are 1.128, 11.283, and 4.442 μm , respectively. The minimum, maximum, and average grain sizes at P2 are 1.128, 9.027, and 4.220 μm , respectively. The minimum, maximum, and average grain

boundary misorientations at P1 are 5.947 $^\circ$, 60.876 $^\circ$, and 39.982 $^\circ$, respectively. The minimum, maximum, and average grain boundary misorientations at P2 are 8.037 $^\circ$, 59.435 $^\circ$, and 41.022 $^\circ$, respectively. The grain sizes and grain boundary

misorientations at P1 and P2 exhibit no significant difference, because the deformation degree is increased with the rotary piercing proceeding. Meanwhile, the inner particles of billet gradually reach the tube wall, and the positions of P1 and P2 are more and more close to each other.

In the whole simulation process of two-high rotary piercing of AZ31 magnesium alloy pipe, the dynamic recrystallization occurs. New grains are formed at the grain boundaries of the original grains, then grow slowly, and finally replace the original grains. This process is repeated continuously. With the rotary piercing proceeding, the distortion of metal crystal structure is accumulated, which provides favorable conditions for the initiation of recrystallization. According to Fig. 7, as the dislocations on the slip plane are inhibited in local areas, the slip is hindered and the recrystallization nucleation occurs near the boundary of the grains and the twins^[14,15]. As shown in Fig. 6–Fig. 9, the transformation of grains from the original massive structure to the strip structure is obvious. With increasing the deformation degree, almost all grains become equiaxed at the end of the piercing.

With the continuous deformation, the recrystallization structures are also increased constantly. The generated grains at the boundaries and in the original grains begin to grow, and gradually replace the original grains. In the end of the deformation process, most microstructures of the AZ31 alloy pipe are renewed after recrystallization, and the grains are very fine. However, it can be observed from Fig. 11 that the grain size is not uniform, due to the uneven heating of the pipe or the rapid heat dissipation of the billet caused by the contact between the roll and the billet. Therefore, the temperature in some positions is too low to obtain a large number of precipitated phases.

3.2 Comparison between experiment and simulation results

To verify the feasibility of simulation results, the simulation results are compared with the experiment results based on

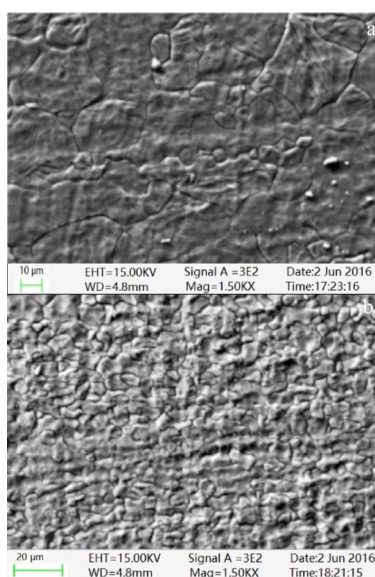


Fig.12 Microstructures of AZ31 magnesium alloys before (a) and after (b) piercing^[6]

Ref. [6]. Fig. 12 shows the microstructures of the AZ31 magnesium alloys before and after the rotary piercing. The experiment average grain sizes before and after piercing are 30 and 3 μm , respectively, which are close to the simulated ones (24.984 and 4.442 μm). In addition, the experimental and simulated microstructure evolution rules are basically the same, indicating the accuracy of simulation results.

4 Conclusions

1) The grain refinement mechanisms of AZ31 magnesium alloy pipe during the two-high rotary piercing process are continuous dynamic recovery and recrystallization. During the deformation, a large number of dislocations are intertwined with each other and finally form the subgrain boundaries and dislocation interfaces. With the rotary piercing proceeding, the dislocations are gradually increased, and the grain boundary misorientation is increased. Subsequently, the low-angle grain boundaries and high-angle grain boundaries are formed, and finally the new recrystallized grains are formed.

2) The simulation results are in good agreement with the experiment results in aspects of grain size, grain shape, and microstructure evolution rule, suggesting the accuracy of simulation results. Thus, the two-high rotary piercing method is suitable for the production of seamless magnesium alloy pipe.

References

- 1 Ding Wenjiang. *Science and Technology of Magnesium Alloy* [M]. Beijing: Science Press, 2007 (in Chinese)
- 2 Zhang Dingfei, Peng Jian, Ding Peidao et al. *Materials Reports* [J], 2004, 18(4): 72 (in Chinese)
- 3 Gou Yujun. *Thesis for Master*[D]. Taiyuan: Taiyuan University of Science and Technology, 2016 (in Chinese)
- 4 Guo Lafeng, An Xiaohong, Lu Liquan et al. *Journal of Plasticity Engineering*[J], 2018, 25(3): 115 (in Chinese)
- 5 Lin Weilu. *Thesis for Master*[D]. Taiyuan: Taiyuan University of Science and Technology, 2018 (in Chinese)
- 6 Ding Xiaofeng, Shuang Yuanhua, Wang Qinghua et al. *Rare Metal Materials and Engineering*[J], 2018, 47(1): 357 (in Chinese)
- 7 Sun Dongfang. *Thesis for Master*[D]. Taiyuan: Taiyuan University of Science and Technology, 2019 (in Chinese)
- 8 Cheng Haitao, Li Chibo, Li Xiao. *Steel Pipe*[J], 2018, 47(5): 78 (in Chinese)
- 9 Ding Xiaofeng. *Thesis for Doctorate*[D]. Taiyuan: Taiyuan University of Science and Technology, 2018 (in Chinese)
- 10 Zhang Baoren. *Thesis for Master*[D]. Hengyang: University of South China, 2013 (in Chinese)
- 11 Zhuang Bo. *Thesis for Master*[D]. Xi'an: Xi'an University of Architecture and Technology, 2017 (in Chinese)
- 12 Incropera F P. *Fundamentals of Heat and Mass Transfer*[M]. Beijing: Chemical Industry Press, 2007 (in Chinese)
- 13 Hu Jianjun, Li Xiaoping. *Deform-3D Plastic Forming CAE Application Course*[M]. Beijing: Peking University Press, 2012

- (in Chinese)
- 14 Chu Zhibing, Zhang Duo, Jiang Lianyun et al. *Rare Metal Materials and Engineering*[J], 2018, 47(3): 884 (in Chinese)
- 15 Chu Zhibing, Wang Huangzhu, Zhang Duo et al. *Rare Metal Materials and Engineering*[J], 2019, 48(10): 3195 (in Chinese)

AZ31 镁合金管二辊斜轧穿孔微观组织演变数值模拟分析

胡建华¹, 梁晓媛², 丁小凤³, 双远华¹, 王清华⁴

(1. 太原科技大学 材料科学与工程学院, 山西 太原 030024)

(2. 西北工业大学 材料学院, 陕西 西安 710072)

(3. 太原科技大学 山西省冶金设备设计理论与技术重点实验室, 山西 太原 030024)

(4. 太原科技大学 电子信息工程学院, 山西 太原 030024)

摘要: 提出了一种镁合金无缝管穿孔新方法 (二辊斜轧穿孔), 并利用三维有限元分析软件 DEFORM-3D 对二辊斜轧穿孔过程进行了模拟, 分析了穿孔过程中的微观组织演变。结果表明, 模拟的微观结构与实验的微观结构具有相同的演变规律, 平均晶粒尺寸接近, 证明了采用二辊穿孔新工艺穿制 AZ31 大口径镁合金无缝管的可行性和 DEFORM-3D 软件模拟结果的可靠性。

关键词: 镁合金无缝管; 二辊穿孔; 数值模拟; 微观组织演变

作者简介: 胡建华, 女, 1977 年生, 博士, 副教授, 太原科技大学材料科学与工程学院, 山西 太原 030024, E-mail: 2005022@tyust.edu.cn